

Getting Dynamic Line Ratings into Markets

Zhiyi Zhou, Christoph Graf, and Yury Dvorkin

Abstract—Static transmission line ratings may lead to underutilization of line capacity due to overly conservative (worst-case) assumptions. Grid-enhancing technologies (GETs) such as dynamic line ratings (DLRs), which adjust line capacity based on real-time conditions, are a techno-economically viable alternative to increase the utilization of existing power lines. Nonetheless, their adoption has been slow, partly due to the absence of operational tools that effectively account for simultaneous impacts on dispatch and pricing. In this paper, we represent transmission capacity with DLRs as a stock-like resource with time-variant interdependency, which is modeled via an approximation of line temperature evolution process, decoupling the impacts of ambient weather conditions and power flow on transmission line temperature and thus capacity. We integrate DLRs into a multi-period DC optimal power flow problem, with chance constraints addressing correlated uncertainty in DLRs and renewable generation. This yields non-convex problems that we transform into a tractable convex form by linearization. We derive locational marginal energy and ancillary services prices consistent with a competitive equilibrium. Numerical experiments on the 11-zone and 1814-node NYISO systems demonstrate its performance, including impacts on dispatch, pricing, and marginal carbon emissions.

I. INTRODUCTION

The backbone transmission system was not originally designed for distributed and intermittent generation, and while this generation may alleviate congestion in some areas, it may also impose new constraints. Transmission congestion costs in the US raised to \$11.5 billion in 2023 [1]. In 2024, CAISO alone curtailed 3.2 million MWh of renewable generation due to transmission constraints [2]. More recently, in addition to challenges from renewable integration, large loads (e.g., data centers and hydrogen electrolyzers) have also begun to contribute to congestion. The commonly used static line ratings (SLRs), which are conservatively derived for worst-case assumptions, are shown to underutilize transmission infrastructure up to 30% even under favorable operational conditions [3]. This highlights the need to safely leverage transmission flexibility to enhance utilization of existing transmission infrastructures.

Dynamic line ratings (DLRs) have emerged as a promising grid-enhancing technology (GET) to increase existing transmission capacity without new line construction, which is time-consuming and capital intensive. DLRs adjust line ratings based on real-time weather conditions, and have moved beyond the pilot stage in many countries, becoming part of standard grid operations. The Oncor Electric Delivery Company achieved up to 12% annual average increases in transmission capacity, which peaked at 30% under favorable conditions [4]. Similarly, DLR implementation on critical corridors in NYPA yielded capacity increases of up to 15% during winter [5]. In Europe, the FLEXITRANSTORE project across six countries increased cross-border transmission capacity by up to 20% [6].

While international adoption has advanced—particularly in systems with system-wide/zonal pricing—nodal markets in the US may present barriers to broader DLR integration, along with several other limiting factors: (a) implementation complexity requiring sophisticated monitoring and control systems [7]; (b) reliability concerns due to uncertainty during high-demand periods [8]; (c) insufficient or misaligned economic incentives under current market structures to justify the investment [9].

While SLRs inaccurately approximate the actual transmission capacity, which in turn hinders economic, reliability, and environmental gains [1], moving to DLRs also requires changes to electricity pricing, which guides investment and operational decisions. Locational marginal pricing (LMP) remains one of the predominant approaches in organized electricity markets [10], composed with the price for energy, transmission congestion, and transmission losses. These prices are derived from the market-clearing model, which usually use a linear DC approximation. Notably, DLRs will affect the congestion component directly and the loss and energy components indirectly. By adding time-varying capacity, DLRs introduce new sources of variability into nodal prices, which calls for more advanced methods of uncertainty management. Existing approaches to manage uncertainty focus on the demand and renewable generation and include scenarios [11], robust [12], and chance constraints (CC) [13]. CC methods align with industry practices, providing transparent risk management without excessive conservatism of deterministic approaches with fixed security margins. Studies [14] and [15] considered the uncertainty in DLRs computations, but ignored important correlations between DLRs and renewable generation. Ignoring weather conditions, i.e. wind speed and direction, which impact both DLRs and wind generation, may lead to suboptimal dispatch. Prior work [16] developed electricity pricing with CC, but without considering DLRs.

This paper models transmission flexibility, enabled by DLRs, and integrates it with electricity pricing. Unlike previous models, i.e. with SLRs [17], DLRs [18], steady-state temperature assumptions underlying transmission line limits [19], the proposed DLR model reflects the influence of multi-period weather conditions on operator’s decisions.

The main contributions of this paper are as follows:

- To incorporate DLRs into routines used for power system and market operations, this paper approximates transmission line temperature evolution and itemizes the contributions of ambient weather conditions and power flow to DLR computations under uncertainty. Through linearization, we represent the uncertain state variables, i.e. line temperature and power flow, as affine functions of optimal power flow (OPF) decisions, which relate the uncertain system states to control inputs.

- Based on this approximation, this paper incorporates DLRs into the multi-period CC DC-OPF, which accounts for the correlation between transmission and wind generation.
- This paper adopts marginal cost-based electricity pricing and considers reserve deliverability under DLRs. We also prove electricity market equilibrium with DLRs and analyze the versatile impacts of DLRs on marginal electricity and reserve prices and marginal emission rates.

II. UNCERTAINTY-AWARE TRANSMISSION FLEXIBILITY

A. DLRs and transmission flexibility

DLRs are computed based on current ambient conditions (e.g. wind speed, wind direction, ambient temperature, and solar radiation) and conductor properties (e.g. diameter, material, and resistor). This relationship is driven by the steady-state heating balance equation:

$$q_c(T_c) + q_r(T_c) = q_s + q_J(T_c, f_c), \quad (1)$$

where q_c and q_r denote convection and radiated heat losses, both dependent on conductor temperature T_c , q_s is solar heat gain, q_J is Joule heat gain determined by temperature T_c and line flow f_c . Using (1), we express f_c as a function of T_c and weather conditions W as $f_c = g(T_c|W)$. Then, DLRs are set based on maximum temperature T_c^{\max} :

$$f_c^{\max} = g(T_c^{\max}|W), \quad (2)$$

where $g(\cdot)$ denotes the mapping from T_c^{\max} to f_c^{\max} under given ambient conditions W at a steady-state equilibrium. The detailed formulation for $g(\cdot)$ is available in Appendix A.

Thermal transient process of a transmission line will last up to 30 minutes [20]. This thermal inertia enables the power flow to temporarily exceed its deterministic rating f_c^{\max} derived in (2), without causing the conductor temperature to surpass its upper limit T_c^{\max} . To capture this effect, we further consider the transient heating balance, assuming that weather conditions remain known in each time period:

$$q_c(T_c) + q_r(T_c) + C \frac{dT_c}{dt} = q_s + q_J(T_c, f_c), \quad (3)$$

where C denotes the total heat capacity of the conductor.

However, since in expression (3), T_c is defined implicitly and cannot be expressed in a closed-form expression, which obstructs modeling an explicit upper bound $T_c \leq T_c^{\max}$ as a constraint in the OPF problem. Instead, we derive the following approximation in Theorem 1:

Theorem 1. Conservative temperature evolution based on transient heating balance. Consider the model in (3). Let the current ambient conditions (e.g. wind speed, wind direction, ambient temperature, and solar radiation) and conductor parameters (e.g. diameter, resistor) satisfy:

$$\Delta r \frac{\partial F_1(\Delta r, \Delta s)}{\partial \Delta r} + \Delta s \frac{\partial F_1(\Delta r, \Delta s)}{\partial \Delta s} < 0 \quad (4a)$$

$$\Delta T \frac{\partial F_2(\Delta T, \Delta I)}{\partial \Delta T} + \Delta I \frac{\partial F_2(\Delta T, \Delta I)}{\partial \Delta I} < 0, \quad (4b)$$

where Δr is a small term associated with q_r , which depends on T_c and ambient conditions W ; Δs is a small term related

with q_s ; $F_1(\Delta r, \Delta s)$ quantifies the residual in (1) resulting from the omission of Δr and Δs , $\Delta T = T_c^{\max} - T_c$ is the difference of the maximum temperature and actual temperature, $\Delta I = \frac{f_c^{\max} - f_c}{V_c}$ is the difference of the maximum current and actual current and V_c is the voltage magnitude; $F_2(\Delta T, \Delta I)$ characterizes the effect of partially neglecting ΔT and ΔI in q_r and q_J on (3). Then power flow f_t and temperature T_t at time t , and temperature T_{t+1} at time $t+1$ satisfy:

$$T_{t+1} < \mu_t^a + \mu_t^b T_t + \mu_t^c f_t^2 + \mu_t^d f_t^4, \quad (5)$$

where μ_t^a , μ_t^b , μ_t^c and μ_t^d are parameters calculated by both current ambient conditions and conductor parameters. ■

Proof of Theorem 1 is given in Appendix B.

Relative to (5), computing $T'_{t+1} = \mu_t^a + \mu_t^b T_t + \mu_t^c f_t^2 + \mu_t^d f_t^4$ leads to $T_{t+1} < T'_{t+1}$. When we set $T'_{t+1} \leq T^{\max}$, it also holds for the actual T_{t+1} as $T_{t+1} \leq T^{\max}$. Then we can get a conservative mapping function from f_t and T_t to T_{t+1} given weather conditions, decomposing the influences of f_t and T_t . The initial static power flow constraint $f_t \leq f^{\max}$ is transformed into a transient line temperature constraint:

$$T_{t+1} = \mu_t^a + \mu_t^b T_t + \mu_t^c f_t^2 + \mu_t^d f_t^4 \quad (6a)$$

$$T_t \leq T^{\max}, \quad (6b)$$

which ensures thermal security and relates to OPF decisions via variable f_t . By capturing thermal evolution, (6) endows a transmission line with stock-like characteristics, which exhibits intertemporal flexibility. Thus, higher power flows increase T_t , reducing future flow capacity and incurring an opportunity cost. Similarly, when power flows are low enough, i.e., heat gain is less than convection and radiated heat loss, T_t will decrease, with increased future transmission capacity.

B. Correlated wind power and DLR uncertainty

To model DLRs within OPF, we consider correlated wind power and DLR uncertainty. The uncertain wind power generation at node i and DLR for line e at time t are as follows:

$$\hat{w}_{i,t} = w_{i,t} + \omega_{i,t} \quad (7a)$$

$$\hat{f}_{e,t}^{\max} = f_{e,t}^{\max} + \xi_{e,t}, \quad (7b)$$

where $\hat{w}_{i,t}$ and $\hat{f}_{e,t}^{\max}$ denote the stochastic wind generation and DLR, each composed of deterministic forecast ($w_{i,t}$, $f_{e,t}^{\max}$) and additive error ($\omega_{i,t}$, $\xi_{e,t}$).

We consider ambient parameters that affect both DLR and wind power, i.e. wind speed, direction, and temperature, and denote their forecast errors by random variables $\varsigma_{i,t}$. We further assume $\omega_{i,t}$ and $\xi_{e,t}$ are linear combinations of $\varsigma_{i,t}$:

$$\omega_{i,t} = \gamma_{w,i,t}^\top \varsigma_{i,t}, \quad \xi_{e,t} = \gamma_{f,e,t}^\top \varsigma_{e,t}, \quad (8)$$

where $\gamma_{w,i,t}$ and $\gamma_{f,e,t}$ are obtained as gradients:

$$\gamma_{w,i,t} = \nabla_{W_{i,t}} w(W_{i,t}) \quad (9a)$$

$$\gamma_{f,e,t} = \nabla_{W_{e,t}} g(T_c^{\max}, W_{e,t}), \quad (9b)$$

where $W_{e,t}$ denotes the vector of ambient conditions, $w(W_{i,t}) = \frac{1}{2} \rho_{i,t} A v_{i,t}^3$ represents wind power generation with air density $\rho_{i,t}$, rotor swept area A , and wind speed $v_{i,t}$ [21]. Given the covariance matrix Σ_ς among all random variables ς , the joint covariance matrix $\Sigma_{\omega\xi}$ for $\omega_{i,t}$ and $\xi_{e,t}$ is:

$$\Sigma_{\omega\xi,t} = \Gamma_{\omega\xi,t}^\top \Sigma_\varsigma \Gamma_{\omega\xi,t}, \quad (10)$$

where $\Gamma_{\omega\xi,t}$ assembles the corresponding sensitivity vectors in alignment with $\varsigma_{i,t}$ and $\varsigma_{e,t}$:

$$(\Gamma_{\omega\xi,t})_i = \gamma_{w,i,t}, \quad (\Gamma_{\omega\xi,t})_e = \gamma_{w,e,t}. \quad (11)$$

Similarly, the uncertainty in temperature evolution is:

$$\hat{\mu}_{e,t}^{[\cdot]}(\varsigma_{e,t}) = \mu_{e,t}^{[\cdot]} + \gamma_{e,t}^{[\cdot]\top} \varsigma_{e,t}, \quad (12)$$

where $\mu_{e,t}^{[\cdot]}$ denotes DLR parameters in (5), and $[\cdot] \in \{a, b, c, d\}$. The covariance matrix $\Sigma_{\omega\varsigma,t}$ for $\omega_{i,t}$ and $\varsigma_{e,t}$ is:

$$\Sigma_{\omega\varsigma,t} = \Gamma_{\omega\varsigma,t}^\top \Sigma_\varsigma \Gamma_{\omega\varsigma,t}, \quad (13)$$

where $\Gamma_{\omega\varsigma,t}$ arranges the sensitivity vectors $\gamma_{w,i,t}$ in the appropriate columns aligned with $\varsigma_{i,t}$.

Building upon DLR constraints in (6) and uncertainty model in (7a) and (12), we construct a stochastic DLR formulation embedded in a CC framework:

$$\begin{aligned} \hat{T}_{e,t+1} = & \hat{\mu}_{e,t}^a(\varsigma_t) + \hat{\mu}_{e,t}^b(\varsigma_t) \hat{T}_t + \hat{\mu}_{e,t}^c(\varsigma_t) \hat{f}_t^2(\omega) \\ & + \hat{\mu}_{e,t}^d(\varsigma_t) \hat{f}_t^4(\omega) \end{aligned} \quad (14a)$$

$$\mathbb{P}_{\varsigma,\omega}[T_t \leq T^{\max}] \geq 1 - \epsilon, \quad (14b)$$

where (14a) is the extension of (6a) under uncertainty. Eq. (14b) is the temperature constraint under CC. The nonlinearity in both decision and random variables renders the resulting feasibility region non-convex.

C. Approximation of non-convex chance constraints

Non-convex constraints in (14) increase computational complexity of the OPF. To cope with this, we first consider a general non-convex CC optimization:

$$\min_{\hat{x}} \sum_{t=1}^T C_t(\hat{x}_t) \quad (15a)$$

$$\hat{u}_{t+1} = h(\hat{u}_t, \hat{x}_t, \phi_t + \varphi_t), t = 1, \dots, T \quad (15b)$$

$$\mathbb{P}_\varphi[q(\hat{u}_t, \hat{x}_t) \leq 0] \geq 1 - \epsilon, t = 1, \dots, T, \quad (15c)$$

where $\hat{x}_t \in \mathbb{R}^n$ denotes the decision variables, corresponding to generator power outputs p_t in the OPF model. The state variables $\hat{u}_t \in \mathbb{R}^m$ are not directly controllable but evolve according to dynamics in (15b). The uncertainty term $\phi_t + \varphi_t$ corresponds to the wind generation and DLR uncertainty expressions in (7a) and (12). For analytical tractability, we assume that $q(u, x)$ is non-decreasing.

In the OPF context, u_t corresponds to f_t and T_t , as described by (14a) and the following equation:

$$f_{e,t} = \sum_{i \in \mathcal{V}} S_{e,i}(p_{i,t} + w_{i,t} - d_{i,t}), \quad (16)$$

where $p_{i,t}$, $d_{i,t}$ and $w_{i,t}$ represent, respectively, the generator power output, load, and wind generation at node i . S is the PTDF matrix for the whole system.

First, consider a deterministic problem ignoring φ_t :

$$\min_x \sum_{t=1}^T C_t(x_t) \quad (17a)$$

$$u_{t+1} = h(u_t, x_t, \phi_t), t = 1, \dots, T \quad (17b)$$

$$q(u_t, x_t) \leq 0, t = 1, \dots, T. \quad (17c)$$

Define $\mathbf{X}_{t+1} = [u_{t+1}, u_t, x_t, \phi_t]^\top$ and let $\mathcal{T}(\mathbf{X}_{t+1}) = 0$ represent (17b). A first-order Taylor approximation at reference point $\check{\mathbf{X}}_{e,t+1} = [\check{u}_{t+1}, \check{u}_t, \check{x}_t, \check{\phi}_t]^\top$ yields:

$$\begin{aligned} \mathcal{T}(\mathbf{X}_{t+1}) = & \mathcal{T}(\check{\mathbf{X}}_{t+1}) + \mathcal{J}(\check{u}_{t+1})(u_{t+1} - \check{u}_{t+1}) \\ & + \mathcal{J}(\check{u}_t)(u_t - \check{u}_t) + \mathcal{J}(\check{x}_t)(x_t - \check{x}_t) \\ & + \mathcal{J}(\check{\phi}_t)(\phi_t - \check{\phi}_t) = 0, \end{aligned} \quad (18)$$

where $\mathcal{J}(\cdot)$ denotes the Jacobian of \mathcal{T} , i.e. partial derivatives relative to its arguments. Since $\mathcal{T}(\check{\mathbf{X}}_{t+1}) = 0$, (18) simplifies to:

$$u_{t+1} = \kappa_t^0 + \kappa_t^u u_t + \kappa_t^x x_t + \kappa_t^\phi \phi_t, \quad (19)$$

where $\kappa_t^0 = \check{u}_{t+1} + \frac{\mathcal{J}(\check{u}_t)}{\mathcal{J}(\check{u}_{t+1})} \check{u}_t + \frac{\mathcal{J}(\check{x}_t)}{\mathcal{J}(\check{u}_{t+1})} \check{x}_t$, $\kappa_t^u = -\frac{\mathcal{J}(\check{u}_t)}{\mathcal{J}(\check{u}_{t+1})} u_t$, $\kappa_t^x = -\frac{\mathcal{J}(\check{x}_t)}{\mathcal{J}(\check{u}_{t+1})} x_t$, $\kappa_t^\phi = -\frac{\mathcal{J}(\check{\phi}_t)}{\mathcal{J}(\check{u}_{t+1})} \phi_t$.

We now incorporate uncertainty φ_t into the equation $h(\cdot)$ in (17b), leading to:

$$\mathcal{T}(\hat{\mathbf{X}}_{t+1}) = \mathcal{T}(\hat{u}_{t+1}, \hat{u}_t, \hat{x}_t, \phi_t + \varphi_t) = 0. \quad (20)$$

Applying a first-order Taylor expansion at the same nominal point $\check{\mathbf{X}}_{e,t+1} = [\check{u}_{t+1}, \check{u}_t, \check{x}_t, \check{\phi}_t]^\top$, we obtain:

$$\hat{u}_{t+1} = \kappa_t^0 + \kappa_t^u \hat{u}_t + \kappa_t^x \hat{x}_t + \kappa_t^\phi (\phi_t + \varphi_t). \quad (21)$$

Combining (19) and (21), the difference between the stochastic and deterministic state becomes:

$$\hat{u}_{t+1} - u_{t+1} = \kappa_t^u (\hat{u}_t - u_t) + \kappa_t^x (\hat{x}_t - x_t) + \kappa_t^\phi \varphi_t, \quad (22)$$

which indicates that \hat{u}_{t+1} depends on all prior uncertainty realizations $\{\varphi_1, \dots, \varphi_t\}$. To manage this propagation, we introduce non-negative auxiliary reserve variables R_t^u and R_t^x as upper bounds on deviations of $\hat{u}_t - u_t$ and $\hat{x}_t - x_t$:

$$R_t^u \geq \max\{\hat{u}_t - u_t, 0\} \quad (23a)$$

$$R_t^x \geq \max\{\hat{x}_t - x_t, 0\} \quad (23b)$$

$$R_{t+1}^u \geq \kappa_t^u R_t^u + \kappa_t^x R_t^x + \kappa_t^\phi \varphi_t. \quad (23c)$$

We thus reformulate the original CC problem as:

$$\min_x \sum_{t=1}^T C_t(x_t + R_t^x) \quad (24a)$$

$$u_{t+1} = \kappa_t^0 + \kappa_t^u u_t + \kappa_t^x x_t + \kappa_t^\mu \mu_t \quad (24b)$$

$$R_1^u = 0 \quad (24c)$$

$$g(u_t + R_t^u, x_t + R_t^x) \leq 0 \quad (24d)$$

$$\mathbb{P}_\varphi[R_{t+1}^u \geq \kappa_t^u R_t^u + \kappa_t^x R_t^x + \kappa_t^\mu \varphi_t] \geq 1 - \epsilon, \quad (24e)$$

where the reformulated CC in (24e) is linear and convex, allowing tractable solution methods under various distributional assumptions on φ_t . We then apply the reformulation in (24) to DLRs in Section III-B.

III. PRICING WITH DLRs

A. Single-period formulation

We first incorporate the steady-state DLR model in (2) into a CC DC-OPF model. Let $\omega = (\omega_1, \dots, \omega_n) \sim \mathcal{N}(0, \Sigma_\omega)$, $\Omega = \sum_{i=1}^n \omega_i$, $\xi_e \sim \mathcal{N}(0, \sigma_{le})$, the vector $b_{\omega e}$ contains covariances, where $b_{\omega e, k} = \text{Cov}(\omega_k, \xi_e)$. The generator output under uncertainty is modeled using a proportional control law as in [13] as $g_i(\Omega) = p_i + \alpha_i \Omega$, where α_i is the participation

factor linking the system-wide wind power imbalance Ω to generator i 's adjustment. The CC DC-OPF is formulated as:

$$\min_{\{p_i, \alpha_i\}} \mathbb{E}_{\omega, \xi} \left[\sum_{i \in \mathcal{G}} c_{i,1} (p_i + \alpha_i \Omega) + c_{i,2} (p_i + \alpha_i \Omega)^2 \right] \quad (25a)$$

$$(\lambda^{\text{bal}}) : \sum_{i \in \mathcal{G}} p_i + \sum_{i \in \mathcal{W}} w_i - \sum_{i \in \mathcal{V}} d_i = 0 \quad (25b)$$

$$(\lambda^\alpha) : \sum_{i \in \mathcal{G}} \alpha_i = 1 \quad (25c)$$

$$(\lambda_i^{\bar{p}}) : p_i + R_i^{\text{up}} \leq p_i^{\text{max}} \quad (25d)$$

$$(\lambda_i^{\underline{p}}) : p_i - R_i^{\text{dn}} \geq p_i^{\text{min}} \quad (25e)$$

$$(\lambda_i^{\text{reo}}) : \mathbb{P}_\omega [\alpha_i \Omega \leq R_i^{\text{up}}] \geq 1 - \epsilon, \forall i \in \mathcal{G} \quad (25f)$$

$$(\lambda_i^{\text{reo}}) : \mathbb{P}_\omega [-\alpha_i \Omega \leq R_i^{\text{dn}}] \geq 1 - \epsilon, \forall i \in \mathcal{G} \quad (25g)$$

$$(\lambda_e^{\bar{F}_0}) : \mathbb{P}_{\omega, \xi} \left[\sum_{i \in \mathcal{V}} S_{e,i} (p_i + w_i - d_i + \alpha_i \Omega - \omega_i) \right. \\ \left. \leq f_e^{\text{max}} + \xi_e \right] \geq 1 - \epsilon, \forall e \in \mathcal{E} \quad (25h)$$

$$(\lambda_e^{\underline{F}_0}) : \mathbb{P}_{\omega, \xi} \left[\sum_{i \in \mathcal{V}} S_{e,i} (p_i + w_i - d_i + \alpha_i \Omega - \omega_i) \right. \\ \left. \geq -f_e^{\text{max}} - \xi_e \right] \geq 1 - \epsilon, \forall e \in \mathcal{E}, \quad (25i)$$

where R_i^{up} and R_i^{dn} represent the up and down reserves for generator i in response to uncertainty Ω . λ is the dual variable corresponding to each constraint. CC (25d) and (25e) enforce generator capacity limits with probability of at least $1 - \epsilon$, while CC (25h) and (25i) limit the probability of overloaded transmission line to ϵ , with the reserve deliverability of $\alpha_i \Omega$ taken into account.

We use a second-order cone (SOC) reformulation [13] to transform the CC-OPF (25) into a deterministic model:

$$\min_{\{p_i, \alpha_i\}} \sum_{i \in \mathcal{G}} c_{i,2} [p_i^2 + \Sigma_\Omega \alpha_i^2] + c_{i,1} p_i \quad (26a)$$

$$\alpha_i \geq 0, (25b), (25c), (25d), (25e)$$

$$(\lambda_i^{\bar{r}}) : R_i^{\text{up}} \geq \Sigma_\Omega^{1/2} \delta \alpha_i, \quad \forall i \in \mathcal{G} \quad (26b)$$

$$(\lambda_i^{\underline{r}}) : R_i^{\text{dn}} \geq \Sigma_\Omega^{1/2} \delta \alpha_i, \quad \forall i \in \mathcal{G} \quad (26c)$$

$$(\lambda_e^{\bar{F}}) : \delta \left\| \left[\frac{\Sigma_\omega^{1/2} (\tilde{S}_e \alpha - \hat{S}_e - \Sigma_\omega^{-1} b_{\omega e})}{\sqrt{\sigma_{le}^2 - b_{\omega e}^\top \Sigma_\omega^{-1} b_{\omega e}}} \right] \right\|_2 \leq \\ -f_e^{\text{max}} - \sum_{i \in \mathcal{V}} S_{e,i} (p_i + w_i - d_i) \quad (26d)$$

$$(\lambda_e^{\underline{F}}) : \delta \left\| \left[\frac{\Sigma_\omega^{1/2} (\tilde{S}_e \alpha - \hat{S}_e - \Sigma_\omega^{-1} b_{\omega e})}{\sqrt{\sigma_{le}^2 - b_{\omega e}^\top \Sigma_\omega^{-1} b_{\omega e}}} \right] \right\|_2 \leq \\ f_e^{\text{max}} + \sum_{i \in \mathcal{V}} S_{e,i} (p_i + w_i - d_i), \quad (26e)$$

where $\delta = \Phi^{-1}(1 - \epsilon)$, $\Sigma_\Omega = e^\top \Sigma_\omega e$, \tilde{S}_e and \hat{S}_e are compact forms of the correlated PTDF matrix components:

$$\hat{S}_e = [S_{e,1}, \dots, S_{e,|\mathcal{V}|}]^\top \in \mathbb{R}^{|\mathcal{V}|} \quad (27a)$$

$$\tilde{S}_e = [\hat{S}_e, \dots, \hat{S}_e]^\top \in \mathbb{R}^{|\mathcal{V}| \times |\mathcal{V}|}. \quad (27b)$$

In (26d) and (26e), we impose the condition $b_{\omega e}^\top \Sigma_\omega^{-1} b_{\omega e} \leq \sigma_{le}^2$ to guarantee the non-negativity of the expression under the square root, which captures the variance of the DLR over

line e , with σ_{le}^2 being the intrinsic component and $b_{\omega e}^\top \Sigma_\omega^{-1} b_{\omega e}$ being induced by the correlated wind uncertainty ω . This assumption reflects the physical observation that DLR is more sensitive to local weather variations than to remote ones.

Based on the formulation in (26) and the Lagrangian methods in [13], the LMP and locational marginal reserve price (LMRP) at node i are given by:

$$\text{LMP}_i = \frac{\partial \mathcal{L}}{\partial d_i} = \lambda^{\text{bal}} - \sum_{e \in \mathcal{E}} \left[(\lambda_e^{\bar{F}} - \lambda_e^{\underline{F}}) S_{e,i} \right] \quad (28a)$$

$$\text{LMRP}_i = \frac{\partial \mathcal{L}}{\partial (R_i^{\text{up}} + R_i^{\text{dn}})} = \lambda_i^{\bar{r}} + \lambda_i^{\underline{r}}, \quad (28b)$$

where \mathcal{L} denotes the Lagrangian function of (26). We calculate LMPs by differentiating \mathcal{L} to local demand d_i , and calculate LMRPs from the derivative of \mathcal{L} to reserves $R_i^{\text{up}} + R_i^{\text{dn}}$.

These expressions follow directly from partial KKT conditions. The stationary conditions for p_i , α_i , R_i^{up} and R_i^{dn} are:

$$\frac{\partial \mathcal{L}}{\partial p_i} : c_{i,1} + 2c_{i,2} p_i + \lambda_i^{\bar{p}} - \lambda_i^{\underline{p}} - \lambda^{\text{bal}} + \\ \sum_{e \in \mathcal{E}} \left[(\lambda_e^{\bar{F}} - \lambda_e^{\underline{F}}) S_{e,i} \right] = 0 \quad (29a)$$

$$\frac{\partial \mathcal{L}}{\partial \alpha_i} : \sum_{e \in \mathcal{E}} (\lambda_e^{\bar{F}} - \lambda_e^{\underline{F}}) Q_e^s \delta + 2c_{i,2} \Sigma_\Omega \alpha_i + \\ (\lambda_i^{\bar{r}} + \lambda_i^{\underline{r}}) \Sigma_\Omega^{1/2} \delta - \lambda^\alpha = 0 \quad (29b)$$

$$\frac{\partial \mathcal{L}}{\partial R_i^{\text{up}}} : \lambda_i^{\bar{p}} - \lambda_i^{\bar{r}} = 0 \quad (29c)$$

$$\frac{\partial \mathcal{L}}{\partial R_i^{\text{dn}}} : \lambda_i^{\underline{p}} - \lambda_i^{\underline{r}} = 0, \quad (29d)$$

where

$$Q_e^s = \frac{\Sigma_\omega (\tilde{S}_e \alpha - \hat{S}_e - \Sigma_\omega^{-1} b_{\omega e})}{\left\| \left[\frac{\tilde{S}_e^\top \Sigma_\omega^{1/2} (\tilde{S}_e \alpha - \hat{S}_e - \Sigma_\omega^{-1} b_{\omega e})}{\sqrt{\sigma_{le}^2 - b_{\omega e}^\top \Sigma_\omega^{-1} b_{\omega e}}} \right] \right\|_2}. \quad (30)$$

Then the LMRPs can also be represented as:

$$\text{LMRP}_i = \frac{1}{\Sigma_\Omega^{1/2} \delta} [\lambda_i^\alpha - 2c_{i,2} \Sigma_\Omega \alpha_i - \sum_{e \in \mathcal{E}} (\lambda_e^{\bar{F}} - \lambda_e^{\underline{F}}) Q_e^s \delta], \quad (31)$$

where λ_i^α is reserve balance price, $2c_{i,2} \Sigma_\Omega \alpha_i$ captures the local generator reserve cost, and $\sum_{e \in \mathcal{E}} (\lambda_e^{\bar{F}} - \lambda_e^{\underline{F}}) Q_e^s \delta$ reflects reserve delivery cost.

We now show that the LMP and LMRP formulations in (28a) and (31) lead to a market equilibrium.

Theorem 2. Market equilibrium for single-period OPF. Let $\{p_i^*, \alpha_i^*\}$ be the optimal solution of the problem in (26) and let $\{\pi_i^*, \tau_i^*\}$ be the LMP and LMRP calculated by (28a) and (31) respectively. Then $\{p_i^*, \alpha_i^*, \pi_i^*, \tau_i^*\}$ constitutes a market equilibrium, i.e.:

- The market clears at $\sum_{i \in \mathcal{G}} p_i + \sum_{i \in \mathcal{W}} w_i - \sum_{i \in \mathcal{V}} d_i = 0$ and $\sum_{i \in \mathcal{G}} \alpha_i = 1$
- Each producer maximizes its profit under payment $\Gamma_i = \pi_i^* p_i^* + \tau_i^* \alpha_i^*$ ■

The proof is given in Appendix C. In this equilibrium, the LMPs and LMRPs, as determined by (28) and (31), provide the

correct economic signals such that each generator, behaving as a price taker in a perfectly competitive market, maximizes its individual profit, while the system-level objective of social welfare maximization, as formulated in (26), is simultaneously achieved.

B. Multi-period formulation

We extend (25) to multiple time periods to incorporate the line temperature evolution model and account for the correlated uncertainty of wind generation and DLRs as in (7a) and (12). The multi-period CC-OPF is:

$$\min \mathbb{E}_{\omega, \varsigma} \left[\sum_t \sum_{i \in \mathcal{G}} c_{i,1} (p_{i,t} + \alpha_{i,t} \Omega_{i,t}) + c_{i,2} (p_{i,t} + \alpha_{i,t} \Omega_{i,t})^2 \right] \quad (32a)$$

$$\alpha_{i,t} \geq 0, \forall t, \forall i$$

$$(\lambda_t^{\text{bal}}) : \sum_{i \in \mathcal{G}} p_{i,t} + \sum_{i \in \mathcal{W}} w_{i,t} - \sum_{i \in \mathcal{V}} d_{i,t} = 0, \forall t \quad (32b)$$

$$(\lambda_t^\alpha) : \sum_{i \in \mathcal{G}} \alpha_{i,t} = 1, \forall t \quad (32c)$$

$$(\lambda_{i,t}^{\bar{p}}) : p_{i,t} + R_{i,t}^{\text{up}} \leq p_i^{\text{max}}, \forall i \in \mathcal{G}, \forall t \quad (32d)$$

$$(\lambda_{i,t}^{\underline{p}}) : p_{i,t} - R_{i,t}^{\text{dn}} \leq p_i^{\text{min}}, \forall i \in \mathcal{G}, \forall t \quad (32e)$$

$$(\lambda_{i,t}^{\pi}) : p_{i,t+1} - p_{i,t} + R_{i,t+1}^{\text{up}} + R_{i,t}^{\text{dn}} \leq U_i^{\text{up}}, \forall i \in \mathcal{G}, \forall t \quad (32f)$$

$$(\lambda_{i,t}^{\pi}) : p_{i,t+1} - p_{i,t} - R_{i,t+1}^{\text{dn}} - R_{i,t}^{\text{up}} \geq -U_i^{\text{dn}}, \forall i \in \mathcal{G}, \forall t \quad (32g)$$

$$(\lambda_{i,t}^{\text{rcu}}) : \mathbb{P}_\omega [R_{i,t}^{\text{up}} \geq \alpha_{i,t} \Omega_{i,t}] \geq 1 - \epsilon, \forall i \in \mathcal{G}, \forall t \quad (32h)$$

$$(\lambda_{i,t}^{\text{rcd}}) : \mathbb{P}_\omega [R_{i,t}^{\text{dn}} \geq -\alpha_{i,t} \Omega_{i,t}] \geq 1 - \epsilon, \forall i \in \mathcal{G}, \forall t \quad (32i)$$

$$(\lambda_{e,t}^{f'}) : \hat{f}_{e,t}(\omega_t) = \sum_{i \in \mathcal{V}} S_{e,i} (p_{i,t} + w_{i,t} - d_{i,t} + \alpha_{i,t} \Omega_{i,t} - \omega_{i,t}), \forall e \in \mathcal{E}, \forall t \quad (32j)$$

$$(\lambda_{e,t}^{T'}) : \hat{T}_{e,t+1}(\omega_t, \varsigma_{e,t}) = \hat{\mu}_{e,t}^a(\varsigma_{e,t}) \hat{T}_{e,t}(\omega_{t-1}, \varsigma_{e,t-1}) + \hat{\mu}_{e,t}^b(\varsigma_{e,t}) \hat{f}_{e,t}^2(\omega_t) + \hat{\mu}_{e,t}^c(\varsigma_{e,t}) \hat{f}_{e,t}^4(\omega_t), \forall e \in \mathcal{E} \quad (32k)$$

$$(\lambda_{e,t}^{\bar{T}}) : \mathbb{P}_{\omega, \varsigma} [\hat{T}_{e,t}(\omega_t, \varsigma_{e,t}) \leq T_e^{\text{max}}] \geq 1 - \epsilon, \forall e \in \mathcal{E}, \quad (32l)$$

where (32k) models the temperature evolution process, capturing the combined effects of wind power and DLR uncertainties. As is discussed in Section II, (32k) and (32l) introduce non-convexity. We approximate this chance constraint via linearization and first consider its deterministic form:

$$T_{e,t+1} = \mu_{e,t}^a + \mu_{e,t}^b T_{e,t} + \mu_{e,t}^c f_{e,t}^2 + \mu_{e,t}^d f_{e,t}^4. \quad (33)$$

We denote (33) as $\mathcal{T}(\mathbf{T}_{e,t+1}) = 0$ with $\mathbf{T}_{e,t+1} = [T_{e,t+1}, T_{e,t}, f_{e,t}, \mu_{e,t}^a, \mu_{e,t}^b, \mu_{e,t}^c, \mu_{e,t}^d]^\top$. Then, we apply a first-order Taylor expansion of $\mathcal{T}(\cdot) = 0$ at the reference point $\check{\mathbf{T}}_{e,t+1} = [\check{T}_{e,t+1}, \check{T}_{e,t}, \check{f}_{e,t}, \check{\mu}_{e,t}^a, \check{\mu}_{e,t}^b, \check{\mu}_{e,t}^c, \check{\mu}_{e,t}^d]^\top$, yielding:

$$\mathcal{T}(\mathbf{T}_{e,t+1}) = \mathcal{T}(\check{\mathbf{T}}_{e,t+1}) + \mathcal{J}_{\mathcal{T}}(\check{\mathbf{T}}_{e,t+1})^\top (\mathbf{T}_{e,t+1} - \check{\mathbf{T}}_{e,t+1}) = 0, \quad (34)$$

where $\mathcal{J}_{\mathcal{T}}$ is the Jacobian of \mathcal{T} . Let $\mathbf{U}_{e,t} = [T_{e,t}, f_{e,t}, \mu_{e,t}^a, \mu_{e,t}^b, \mu_{e,t}^c, \mu_{e,t}^d]^\top$, $\kappa_{e,t+1} = \frac{\mathcal{J}_{\mathcal{T}}(\check{\mathbf{U}}_{e,t})}{\mathcal{J}_{\mathcal{T}}(\check{\mathbf{T}}_{e,t+1})}$, $\kappa_{e,t+1}^a = \mathcal{J}_{\mathcal{T}}(\check{\mathbf{T}}_{e,t+1})$. Since $\mathcal{T}(\check{\mathbf{T}}_{e,t+1}) = 0$, (34) can be:

$$T_{e,t+1} = \kappa_{e,t+1}^a + \kappa_{e,t+1}^\top \mathbf{U}_{e,t}. \quad (35)$$

Using (35), (32k) can be linearized as:

$$\hat{T}_{e,t+1} = \kappa_{e,t+1}^a + \kappa_{e,t+1}^\top \hat{\mathbf{U}}_{e,t}(\omega_t, \varsigma_{e,t}), \quad (36)$$

where $\hat{\mathbf{U}}_{e,t} = [\hat{T}_{e,t}, \hat{f}_{e,t}, \hat{\mu}_{e,t}^a, \hat{\mu}_{e,t}^b, \hat{\mu}_{e,t}^c, \hat{\mu}_{e,t}^d]^\top$.

According to (32j), the stochastic variable $\hat{f}_{e,t}(\omega_t)$ can be reformulated according to deterministic value $f_{e,t}$ as:

$$\begin{aligned} \hat{f}_{e,t}(\omega_t) &= f_{e,t} + \sum_{i \in \mathcal{V}} S_{e,i} (\alpha_{i,t} \sum_{j \in \mathcal{W}} \omega_{j,t} - \omega_{i,t}) \\ &= f_{e,t} + \kappa_{e,t} \alpha_t \omega_t, \end{aligned} \quad (37)$$

where $\kappa_{e,t}$ is a matrix to transform $\sum_{i \in \mathcal{V}} S_{e,i} (\alpha_{i,t} \sum_{j \in \mathcal{W}} \omega_{j,t} - \omega_{i,t})$ into $\kappa_{e,t} \alpha_t \omega_t$ for simplicity.

Denote $\mu_{e,t} = [\mu_{e,t}^a, \mu_{e,t}^b, \mu_{e,t}^c, \mu_{e,t}^d]^\top$, $\kappa_{e,t+1}^\mu = \frac{\mathcal{J}_{\mathcal{T}}(\check{\mu}_{e,t})}{\mathcal{J}_{\mathcal{T}}(\check{\mathbf{T}}_{e,t+1})}$, $\kappa_{e,t+1}^b = \frac{\mathcal{J}_{\mathcal{T}}(\check{T}_{e,t})}{\mathcal{J}_{\mathcal{T}}(\check{\mathbf{T}}_{e,t+1})}$, $\kappa_{e,t+1}^c = \frac{\mathcal{J}_{\mathcal{T}}(\check{f}_{e,t})}{\mathcal{J}_{\mathcal{T}}(\check{\mathbf{T}}_{e,t+1})}$. Combine (12) and (37) with (36), we can get:

$$\begin{aligned} \hat{T}_{e,t+1} - T_{e,t+1} &= \kappa_{e,t+1}^b (\hat{T}_{e,t} - T_{e,t}) + \kappa_{e,t+1}^c \kappa_{e,t} \alpha_t \omega_t \\ &\quad + \kappa_{e,t+1}^{\mu \top} \gamma_{e,t} \varsigma_{e,t} \\ &= \kappa^b (\hat{T}_{e,t} - T_{e,t}) + \kappa^c \alpha_t \omega_t + \kappa^d \varsigma_{e,t}, \end{aligned} \quad (38)$$

where $\gamma_{e,t} = \text{diag}\{\gamma_{e,t}^a, \gamma_{e,t}^b, \gamma_{e,t}^c, \gamma_{e,t}^d\}$, $\kappa^c = \kappa_{e,t+1}^c \kappa_{e,t}$, $\kappa^d = \kappa_{e,t+1}^{\mu \top} \gamma_{e,t}$. Since $\hat{T}_{e,t+1}$ depends on $\{\omega_1, \dots, \omega_t, \varsigma_1, \dots, \varsigma_t\}$, we introduce the auxiliary thermal reserve $R_{e,t}^{\text{th}}$ to relax $\hat{T}_{e,t} - T_{e,t}$:

$$\begin{aligned} R_{e,t+1}^{\text{th}} &= \max_{\omega, \varsigma} \left\{ \hat{T}_{e,t+1} - T_{e,t+1} \right\} \\ &= \max_{\omega, \varsigma} \left\{ \kappa^b (\hat{T}_{e,t} - T_{e,t}) + \kappa^c \alpha_t \omega_t + \kappa^d \varsigma_{e,t} \right\} \\ &= \kappa^b R_{e,t}^{\text{th}} + \kappa^c \alpha_t \omega_t + \kappa^d \varsigma_{e,t}. \end{aligned} \quad (39)$$

Note that this auxiliary thermal reserve $R_{e,t}^{\text{th}}$ represents the spare transmission capacity and is not related to the primary/secondary/tertiary reserve products for frequency and contingencies. This thermal reserve is introduced to solve the combined uncertainty and non-convexity. Then (38) can be relaxed as:

$$R_{e,t}^{\text{th}} \geq \hat{T}_{e,t} - T_{e,t} \quad (40a)$$

$$\begin{cases} R_{e,1}^{\text{th}} = 0 \\ R_{e,t+1}^{\text{th}} \geq \kappa^b R_{e,t}^{\text{th}} + \kappa^c \alpha_t \omega_t + \kappa^d \varsigma_{e,t}, \text{ for } t \geq 1. \end{cases} \quad (40b)$$

Then (32j) - (32l) can be replaced by:

$$(\lambda_{e,t}^f) : f_{e,t} = \sum_{i \in \mathcal{V}} S_{e,i} (p_{i,t} + w_{i,t} - d_{i,t}) \quad (41a)$$

$$\begin{aligned} \mathbb{P}_{\omega, \varsigma} [R_{e,t+1}^{\text{th}} &\geq \kappa^b R_{e,t}^{\text{th}} + \kappa^c \alpha_t \omega_t + \kappa^d \varsigma_{e,t}] \\ &\geq 1 - \epsilon, \forall e \in \mathcal{E}, \forall t \end{aligned} \quad (41b)$$

$$\begin{aligned} (\lambda_{e,t}^T) : T_{e,t+1} &= \kappa^a + \kappa^b T_{e,t} + \kappa^c f_{e,t} + \kappa^d \mu_{e,t}^a \\ &\quad + \kappa^e \mu_{e,t}^b + \kappa^f \mu_{e,t}^c + \kappa^g \mu_{e,t}^d \end{aligned} \quad (41c)$$

$$R_{e,1}^{\text{th}} = 0 \quad (41d)$$

$$(\lambda_{e,t}^{\bar{T}}) : T_{e,t} + R_{e,t}^{\text{th}} \leq T_e^{\text{max}}. \quad (41e)$$

Assume $\varsigma \sim \mathcal{N}(0, \Sigma_\varsigma)$, the vector b_{ω_e} contains covariances, where $b_{\omega_e, k} = \text{Cov}(\omega_k, \varsigma_e)$. Then all chance constraints can be transformed into SOC constraints:

$$(\lambda_{e,t}^{\text{rcu}}) : \Sigma_\Omega^{1/2} \delta \alpha_i \leq R_{i,t}^{\text{up}}, \forall i \in \mathcal{G}, \forall t \quad (42a)$$

$$(\lambda_{e,t}^{\text{rcd}}) : \Sigma_\Omega^{1/2} \delta \alpha_i \leq R_{i,t}^{\text{dn}}, \forall i \in \mathcal{G}, \forall t \quad (42b)$$

$$(\lambda_{e,t}^{\text{th}}) : \delta \left\| \left[\frac{\Sigma_{\omega}^{1/2} \dot{\kappa}^c \alpha_t + \Sigma_{\omega}^{-1/2} \dot{\kappa}^d b_{\omega_e}^{\top}}{\sqrt{\dot{\kappa}^{d\top} \Sigma_{\zeta} \dot{\kappa}^d - b_{\omega_e} \dot{\kappa}^{d\top} \Sigma_{\omega}^{-1} \dot{\kappa}^d b_{\omega_e}^{\top}}} \right] \right\|_2 \leq$$

$$R_{e,t+1}^{\text{th}} - \kappa^b R_{e,t}^{\text{th}}, \forall e \in \mathcal{E}, \forall t, \quad (42c)$$

where $\delta = \Phi^{-1}(1 - \epsilon)$. In (42c), we impose the condition $b_{\omega_e} \dot{\kappa}^{d\top} \Sigma_{\omega}^{-1} \dot{\kappa}^d b_{\omega_e}^{\top} \leq \dot{\kappa}^{d\top} \Sigma_{\zeta} \dot{\kappa}^d$ to ensure the non-negativity of the expression under the square root, which captures the variance of DLR_e, where σ_{ζ}^2 denotes its intrinsic variance, and $b_{\omega_e} \dot{\kappa}^{d\top} \Sigma_{\omega}^{-1} \dot{\kappa}^d b_{\omega_e}^{\top}$ quantifies the contribution from correlated wind uncertainty ω . This assumption reflects the physical observation that DLR is more sensitive to local weather conditions rather than to remote ones.

The initial multi-period CC DC-OPF problem in (32) can be reformulated as:

$$\min_{\mathcal{P}} \sum_t \sum_{i \in \mathcal{G}} c_{i,2} [p_{i,t}^2 + \Sigma_{\Omega} \alpha_{i,t}^2] + c_{i,1} p_{i,t} \quad (43)$$

$$\alpha_{i,t} \geq 0, (32b), (32c), (32d), (32e), (32f), (32g),$$

$$(41a), (41c), (41d), (41e), (42a), (42b), (42c),$$

where $\mathcal{P} = \{p_{i,t}, \alpha_{i,t}, f_{e,t}, T_{e,t}, R_{i,t}^{\text{up}}, R_{i,t}^{\text{dn}}, R_{i,t}^{\text{th}}\}$, and then the reformulated problem (43) is convex.

Using (43), we obtain the LMP and LMRP at node i :

$$\text{LMP}_{i,t} = \frac{\partial \mathcal{L}}{\partial d_{i,t}} = \lambda_t^{\text{bal}} - \sum_{e \in \mathcal{E}} S_{e,i} \lambda_{e,t}^f \quad (44a)$$

$$\text{LMRP}_{i,t} = \frac{\partial \mathcal{L}}{\partial (R_{i,t}^{\text{up}} + R_{i,t}^{\text{dn}})} = \lambda_{i,t}^{\text{re}} + \lambda_{i,t}^{\text{re}}, \quad (44b)$$

which can be derived due to partial KKT conditions:

$$(p_{i,t}) : 2c_{i,2} p_{i,t} + c_{i,1} - \lambda_t^{\text{bal}} + \lambda_{i,t}^{\text{p}} - \lambda_{i,t}^{\text{p}} - \lambda_{i,t}^{\text{r}} + \lambda_{i,t}^{\text{r}} \\ + \lambda_{i,t-1}^{\text{r}} - \lambda_{i,t-1}^{\text{r}} + \sum_{e \in \mathcal{E}} S_{e,i} \lambda_{e,t}^f = 0 \quad (45a)$$

$$(\alpha_{i,t}) : 2c_{i,2} \Sigma_{\Omega} \alpha_{i,t} - \lambda_t^{\alpha} + (\lambda_{i,t}^{\text{re}} + \lambda_{i,t}^{\text{re}}) \Sigma_{\Omega}^{1/2} \delta \\ + \sum_{e \in \mathcal{E}} \lambda_{e,t}^{\text{th}} Q_{e,t}^m \delta = 0 \quad (45b)$$

$$(f_{e,t}) : \lambda_{e,t}^f - \kappa_{e,t}^c \lambda_{e,t}^T = 0 \quad (45c)$$

$$(T_{e,t}) : \lambda_{e,t-1}^T - \kappa_{e,t}^b \lambda_{e,t}^T + \lambda_{e,t}^{\text{th}} = 0, \quad (45d)$$

where $Q_{e,t}^m = \frac{\dot{\kappa}^{c\top} \Sigma_{\omega} \dot{\kappa}^c \alpha_t + \Sigma_{\omega}^{-1} \dot{\kappa}^d b_{\omega_e}^{\top}}{\left\| \left[\frac{\Sigma_{\omega}^{1/2} \dot{\kappa}^c \alpha_t + \Sigma_{\omega}^{-1/2} \dot{\kappa}^d b_{\omega_e}^{\top}}{\sqrt{\dot{\kappa}^{d\top} \Sigma_{\zeta} \dot{\kappa}^d - b_{\omega_e} \dot{\kappa}^{d\top} \Sigma_{\omega}^{-1} \dot{\kappa}^d b_{\omega_e}^{\top}}} \right] \right\|_2}$. Then

we can reformulate the LMPs and LMRPs as:

$$\text{LMP}_{i,t} = \lambda_t^{\text{bal}} - \frac{1}{2} \sum_{e \in \mathcal{E}} S_{e,i} \times$$

$$\left[\kappa_{e,t+1}^b \lambda_{e,t+1}^T - \lambda_{e,t+1}^{\text{th}} + \frac{\lambda_{e,t-1}^T + \lambda_{e,t}^{\text{th}}}{\kappa_{e,t}^b} \right] \quad (46a)$$

$$\text{LMRP}_{i,t} = \frac{1}{\Sigma_{\Omega}^{1/2} \delta} [\lambda_t^{\alpha} - 2c_{i,2} \Sigma_{\Omega} \alpha_{i,t} - \sum_{e \in \mathcal{E}} \lambda_{e,t}^{\text{th}} Q_{e,t} \delta], \quad (46b)$$

which shows that the LMPs at time t are affected by the thermal state and power flow at both time $t - 1$ and time $t + 1$, indicating that LMPs are influenced by the time-varient interdependency introduced by DLRs. In LMPRs, λ_i^{α} is reserve balance price, $2c_{i,2} \Sigma_{\Omega} \alpha_i$ is local generator reserve cost, and $\sum_{e \in \mathcal{E}} \lambda_{e,t}^{\text{th}} Q_{e,t} \delta$ is reserve delivery cost.

We now show that the LMP and LMRP formulations in (44) and (46b) naturally induce a market equilibrium.

Theorem 3. Market equilibrium for single-period OPF.

Let $\{p_{i,t}^*, \alpha_{i,t}^*, f_{e,t}^*, T_{e,t}^*, R_{i,t}^{\text{up}*}, R_{i,t}^{\text{dn}*}, R_{i,t}^{\text{th}*}\}$ be the optimal solution of the problem in (43) and let $\{\pi_i^*, \tau_i^*\}$ be the LMP and LMRP calculated by (44) and (46b) respectively. Then $\{p_{i,t}^*, \alpha_{i,t}^*, f_{e,t}^*, T_{e,t}^*, R_{i,t}^{\text{up}*}, R_{i,t}^{\text{dn}*}, R_{i,t}^{\text{th}*}, \pi_i^*, \tau_i^*\}$ constitutes a market equilibrium, i.e.:

- The market clears at $\sum_{i \in \mathcal{G}} p_{i,t} + \sum_{i \in \mathcal{W}} w_{i,t} - \sum_{i \in \mathcal{V}} d_{i,t} = 0$ and $\sum_{i \in \mathcal{G}} \alpha_{i,t} = 1$
- Each producer maximizes its profit under the payment $\Gamma_i = \sum_t \pi_{i,t}^* p_{i,t}^* + \tau_{i,t}^* \alpha_{i,t}^*$ ■

The proof is given in Appendix D. Theorem 3 implies that, given the LMPs and LMRPs computed from (44) and (46b), each generator, acting as a price taker, maximize its individual profit while the overall social welfare is maximized as formulated in (43).

C. Comparison of LMP and LMRP under different line ratings

Table I summarizes the formulation of LMPs and LMRPs under different line rating models (SLR, DLR, and CC DLR). In both the single- and multi-period settings, the LMP consists of total energy balance price and congestion price characterized by $\sum_{e \in \mathcal{E}} S_{e,i} \lambda_{e,t}^f$. The LMRP reflects the total system reserve balance cost, local generator reserve cost, and reserve delivery cost, which differs depending on the adopted DLR model. For steady-state DLR models in single-period problem, it is expressed using the direct power flow limit as $\sum_{e \in \mathcal{E}} (\lambda_{e,t}^{\text{F}} - \lambda_{e,t}^{\text{F}}) Q_{e,t}^s \delta$, while for transient thermal models, it is expressed in terms of thermal constraints as $\sum_{e \in \mathcal{E}} \lambda_{e,t}^{\text{th}} Q_{e,t}^m \delta$.

TABLE I
COMPARISON OF PRICING OUTCOMES UNDER DIFFERENT LINE RATING MODELS

| Line rating models | Single period OPF | Multi period OPF |
|--------------------|---|---|
| SLR | $\text{LMP}_i = \lambda^{\text{bal}} - \sum_{e \in \mathcal{E}} S_{e,i} \lambda_e^f$ | $\text{LMP}_{i,t} = \lambda_t^{\text{bal}} - \sum_{e \in \mathcal{E}} S_{e,i} \lambda_{e,t}^f$ |
| DLR | $\text{LMP}_i = \lambda^{\text{bal}} - \sum_{e \in \mathcal{E}} S_{e,i} \lambda_e^f$ | $\text{LMP}_{i,t} = \lambda_t^{\text{bal}} - \sum_{e \in \mathcal{E}} S_{e,i} \lambda_{e,t}^f$ |
| Stochastic DLR | $\text{LMP}_i = \lambda^{\text{bal}} - \sum_{e \in \mathcal{E}} S_{e,i} \lambda_e^f$ $\text{LMRP}_i = \frac{\lambda_i^{\alpha}}{\Omega} - 2c_{i,2} \Omega \alpha_i - \sum_{e \in \mathcal{E}} S_{e,i} (\lambda_e^{\text{F}} - \lambda_e^{\text{F}})$ | $\text{LMP}_{i,t} = \lambda_t^{\text{bal}} - \sum_{e \in \mathcal{E}} S_{e,i} \lambda_{e,t}^f$ $\text{LMRP}_{i,t} = \frac{\lambda_t^{\alpha}}{\Omega_t} - 2c_{i,2} \Omega_t \alpha_{i,t} + \sum_{e \in \mathcal{E}} S_{e,i} \lambda_{e,t}^f$ |
| CC DLR | $\text{LMP}_i = \lambda^{\text{bal}} - \sum_{e \in \mathcal{E}} S_{e,i} \lambda_e^f$ $\text{LMRP}_i = \frac{1}{\Sigma_{\Omega}^{1/2} \delta} [\lambda_i^{\alpha} - 2c_{i,2} \Sigma_{\Omega} \alpha_i - \sum_{e \in \mathcal{E}} (\lambda_e^{\text{F}} - \lambda_e^{\text{F}}) Q_{e,t}^s \delta]$ | $\text{LMP}_{i,t} = \lambda_t^{\text{bal}} - \sum_{e \in \mathcal{E}} S_{e,i} \lambda_{e,t}^f$ $\text{LMRP}_{i,t} = \frac{1}{\Sigma_{\Omega}^{1/2} \delta} [\lambda_t^{\alpha} - 2c_{i,2} \Sigma_{\Omega} \alpha_{i,t} - \sum_{e \in \mathcal{E}} \lambda_{e,t}^{\text{th}} Q_{e,t}^m \delta]$ |

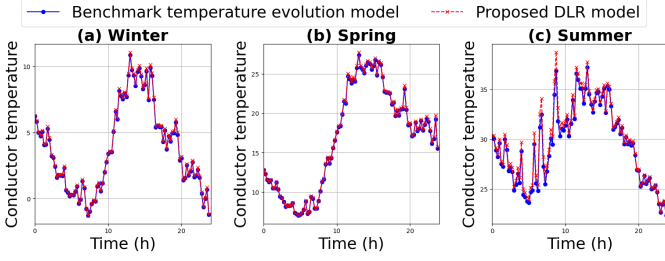


Fig. 1. Line temperature evolution under three seasonal scenarios using the benchmark model (red) and proposed model (blue) in (5)

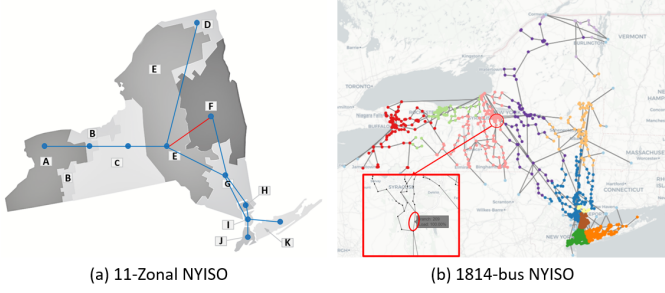


Fig. 2. Zonal and nodal representations of the NYISO system with (a) DLRs on interface E-F; (b) DLRs on Line 206.

TABLE II
THE STATISTIC APPROXIMATION ERROR UNDER THREE SCENARIOS

| Scenario | MAE (°C) | Max Error (°C) |
|-------------|----------|----------------|
| Winter | 0.0950 | 0.2484 |
| Spring/Fall | 0.1359 | 0.5218 |
| Summer | 0.4123 | 1.8684 |

IV. NUMERICAL EXPERIMENTS

A. Approximation of line temperature evolution

We analyze a standard ACSR Drake 795 conductor [22] to compare the proposed approximation in (5) of Theorem 1 and the benchmark method, which obtains temperature evolution numerically via discrete integration over 1-minute intervals [18], [20]. Using 24-hour data sampled at 15-minute intervals, we test typical winter, fall/spring, and summer conditions with varying wind speed/direction, solar radiation, ambient temperatures, and power flows. Fig. 1 displays the comparison, in which our method consistently predicts higher temperatures than the benchmark model, validating that it is a tight and conservative bound. Table II also presents the mean absolute error (MAE) and the maximum error. The summer scenario exhibits the largest MAE (0.4123°C) and the peak error of 1.8684°C at 9 AM, when a relatively high solar radiation coincides with an unusually low wind speed of 1.2 m/s. This is consistent with (61), where terms $\Delta r = \Delta s = 0$ introduce a linearization error amplified by the inverse of convective heat losses (dominated by wind speed), making the proposed approximation less accurate at lower wind speeds.

B. 11-zone NYISO system

1) *Single-day analysis:* We evaluate the proposed multi-period model in (43) using the 11-zonal NYISO system in

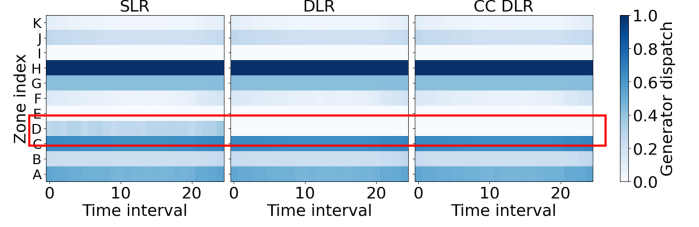


Fig. 3. Optimal dispatch results for the 11-zonal NYISO system: both DLR and CC DLR greatly decrease the higher-cost generation in Zone D compared with SLR cases by alleviating the congestion on line E-F (red box)

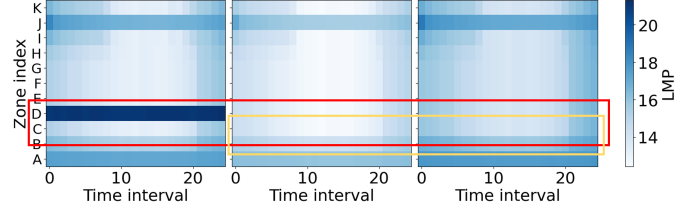


Fig. 4. LMP comparison for the 11-zonal NYISO system: DLR reduces the LMP in Zone D at 5:00 from 19.35 \$/MWh to 13.87 \$/MWh (red box). CC DLR increased the LMP in Zone A at 5:00 from 16.07 \$/MWh to 17.63 \$/MWh (yellow box).

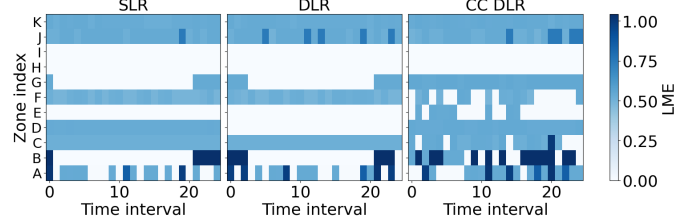


Fig. 5. LME comparison for the 11-zonal NYISO system

Fig.2(a) [23], which includes 12 line interfaces, 361 thermal generators (37.9 GW), and 38 wind farms (6.3 GW primarily in Zones E, G, and K). We model DLRs on the historically congested E-F interface for the typical summer day and compare the following three cases: (a) SLRs; (b) DLRs; (c) CC with DLRs and correlated uncertainty.

Fig. 3-5 summarize the optimal dispatch, LMP and locational marginal emission (LME)¹ results for the three cases. In the SLR case, higher-cost generators in Zone D are marginal due to congestion between zones E-F, preventing the delivery of low-cost electricity from Zone F. DLRs alleviate congestion, reducing more expensive generation in Zone D, leading to the total cost reductions by 0.686% and 0.242% in the DLR and CC-DLR cases. In both DLR cases, DLRs substantially reduce LMP differences between Zones D, E and F. The CC-DLR case maintains a security margin for wind uncertainty and enables more power transfer than static ratings (by 15.38%). Considering correlated uncertainty (CC-DLR case) leads to minor dispatch differences with the DLR case, but more pronounced and bidirectional LMP impacts (see Fig. 4). For instance, the DLR case reduces the LMP in Zone D from 19.35 \$/MWh to 13.87 \$/MWh. However, considering the

¹We compute LMEs by identifying the marginal generator(s) at each node, i.e., if the output (including reserve) is strictly within operational limits. The LME is then determined by the emission rate of the marginal generator(s).

TABLE III
IMPACTS OF DLR AND CC DLR ON SYSTEM COST AND EMISSION
COMPARED TO SLR BASELINE

| Season | Total cost | | Total emission | |
|-------------|------------|--------|----------------|--------|
| | DLR | CC DLR | DLR | CC DLR |
| Spring/Fall | -0.67% | -0.41% | -0.81% | -0.38% |
| Summer | -0.09% | 0.00% | -1.58% | -1.61% |
| Fall | -0.78% | -0.75% | -2.25% | -2.23% |

correlated uncertainty in the CC-DLR case may drive the need for additional transmission reserve margins and, thus, suppress access to some low-cost generation. For example, this raises the LMP in Zone A at 5:00 from 16.07 \$/MWh to 17.63 \$/MWh. The increasing total cost for the CC-DLR case, as compared with the DLR case, arises from the additional reserve provision, which is 5.14 MW in Zone D at 5:00. The corresponding LMRP is 52.77 \$/MWh, higher than LMP since it reflects the opportunity cost and flexibility premium of keeping capacity available. Both DLR cases also reduce the total carbon emissions and, notably, some LMEs - for instance, in Zone D at 5:00 from 0.537 kg/kWh to 0 kg/kWh.

2) *Weighted multi-day analysis*: We use the representative days in Table II to extend the analysis in Section IV-B1. Table III summarizes the changes in total system cost and total emissions under DLR and CC-DLR, relative to the baseline case with SLR, which shows the overall cost emissions and reduction savings. Under all three scenarios, the introduction of DLR increases the LME in Zone E. This is because the original congestion on interface E-F limits wind power export, resulting in full local consumption. With DLR and CC-DLR, the increased E-F capacity enables abundant wind export, and additional demand in Zone E must be met by carbon-emitting thermal units, thereby raising the LME.

C. 1814-node NYISO system

We use the 1814-node NYISO system [24] in Fig. 2(b) to show scalability of the proposed model. This system includes 2208 branches and the same thermal and wind generators as before. DLRs are modeled for frequently congested branch 206 using the summer scenario. Fig. 6 shows that DLRs reduce congestion, enabling production from low-cost generator 71. Fig. 7 and 8 summarize LMPs and LMEs. We list all 106 nodes that host generators out of the total 1814 nodes. LMP differential across the system decreases in the two DLR cases. However, nodal results are again bidirectional, despite the system-wide cost savings and emissions reductions. For example, the LMP at node 74 rises from nearly zero with SLRs to 11.395 \$/MWh with DLRs, while the LMP at node 25 decreases during most periods. Similarly, in Fig. 8, the LMEs generally reduce under DLRs and CC-DLRs, while the total emissions are reduced by 0.20% and 0.24%.

V. CONCLUSION

This paper integrates DLR models based on the approximate line temperature evolution into electricity market optimization tools, capturing the effects of flexible transmission limits and weather conditions on dispatch and market outcomes.

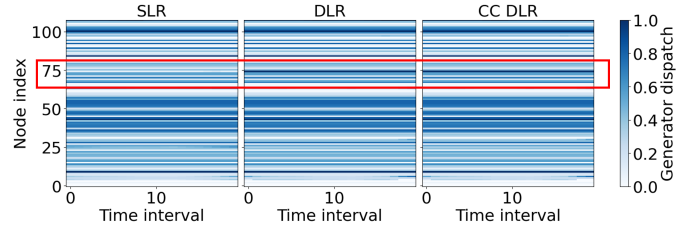


Fig. 6. Optimal dispatch results on 106 nodes with generators for the 1814-node NYISO system: the generator at bus 74 increases from 8.9% to 100% generation with changes between the SLR and DLR cases (red box).

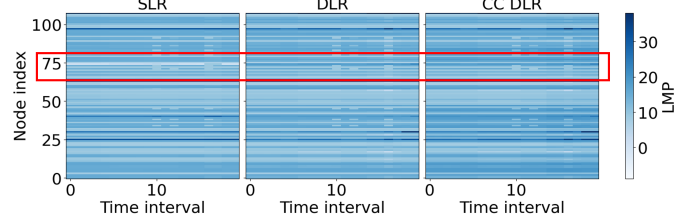


Fig. 7. LMPs on 106 nodes with generators for the 1814-node NYISO system: the LMP at node 74 rises from nearly zero with SLRs to 11.395 \$/MWh with DLRs (red box)

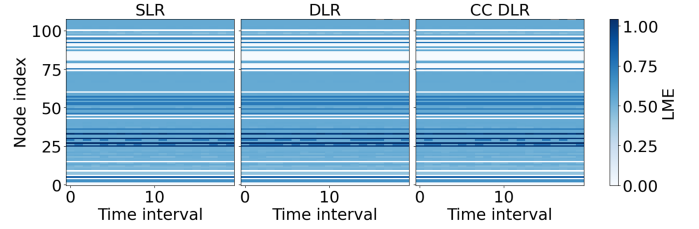


Fig. 8. LMEs on 106 nodes with generators for the 1814-node NYISO system

By replacing traditional constraints with transient thermal constraints, the approach enhances transmission utilization while maintaining system security. To solve the multi-period OPF formulation, convexified chance constraints are developed to address correlated uncertainties in DLRs and wind power. The framework introduces thermal reserves to capture uncertainty impacts on transmission capacity and derives LMPs and LMRPs that support competitive market equilibrium.

Our case study shows, compared with SLRs, DLRs can reduce costs by up to 0.686% (11-zone) and 0.22% (1814-node) while lowering prices in congested areas by up to 28.3% and the total emissions by up to 2.23%. Notably, the choice between zonal and nodal system representations significantly influences cost and emissions outcomes, potentially shaping the deployment and actual benefits of DLRs. Between the zonal and nodal implementations, we do not observe major differences in dispatch decisions, but note that there pronounced impacts in LMPs and LMRPs that may affect revenue opportunities of specific producers.

REFERENCES

- [1] N. Shreve *et al.*, "2023 transmission congestion report," 2024. [Online]. Available: <http://bit.ly/3ZCrMao>
- [2] California ISO, "Managing the evolving grid," <https://tinyurl.com/5xm75wvb>.

- [3] W. Wang and S. Pinter, "Dynamic line rating systems for transmission lines: Topical report," *US Department of Energy*, 2014.
- [4] O. E. D. Company, "Oncor's dynamic line rating (dlr) project," U.S. Department of Energy, Tech. Rep., May 2014. [Online]. Available: <https://tinyurl.com/bdzh4u3a>
- [5] C. C. Xu, "Nypa experience with dynamic line rating technology," New York Power Authority, Tech. Rep., September 2019. [Online]. Available: <https://tinyurl.com/y5wdp5yr>
- [6] ENTSO-E, "Dynamic line rating (dlr). [Online]. Available: <https://tinyurl.com/msnu7hrb>
- [7] E. Fernandez *et al.*, "Review of dlr systems for wind power integration," *Renew. Sustain. Energy Rev.*, vol. 53, pp. 80–92, 2016.
- [8] A. Wilke, "Dlr: A pragmatic approach to implementation," 2024.
- [9] K. W. Cheung, "Ferc order 881-a step towards dynamic line ratings for improved market efficiency," in *2022 IEEE PES 14th Asia-Pac. Power Energy Eng. Conf. (APPEEC)*. IEEE, 2022, pp. 1–6.
- [10] M. Munasinghe, "Principles of modern electricity pricing," *Proceedings of the IEEE*, vol. 69, no. 3, pp. 332–348, 1981.
- [11] A. Papavasiliou *et al.*, "Reserve requirements for wind power integration: A scenario-based stochastic programming framework," *IEEE Trans. Power Syst.*, vol. 26, no. 4, pp. 2197–2206, 2011.
- [12] D. Bertsimas *et al.*, "Adaptive robust optimization for the security constrained unit commitment problem," *IEEE Trans. Power Syst.*, vol. 28, no. 1, pp. 52–63, 2012.
- [13] D. Bienstock *et al.*, "Chance-constrained optimal power flow: Risk-aware network control under uncertainty," *Siam Review*, vol. 56, no. 3, pp. 461–495, 2014.
- [14] N. Viafora *et al.*, "Chance-constrained optimal power flow with non-parametric probability distributions of dynamic line ratings," *Int. J. Electr. Power Energy Syst.*, vol. 114, p. 105389, 2020.
- [15] C. Wang *et al.*, "Risk-based distributionally robust optimal power flow with dynamic line rating," *IEEE Trans. Power Syst.*, vol. 33, no. 6, pp. 6074–6086, 2018.
- [16] Y. Dvorkin, "A chance-constrained stochastic electricity market," *IEEE Trans. Power Syst.*, vol. 35, no. 4, pp. 2993–3003, 2019.
- [17] L. Halilbašić *et al.*, "Convex relaxations and approximations of chance-constrained ac-opf problems," *IEEE Trans. Power Syst.*, vol. 34, no. 2, pp. 1459–1470, 2019.
- [18] B. Xu *et al.*, "Impacts of dynamic line rating on power dispatch performance and grid integration of renewable energy sources," in *IEEE PES ISGT Europe 2013*. IEEE, 2013, pp. 1–5.
- [19] B. O. Ngoko *et al.*, "Optimal power flow considering line-conductor temperature limits under high penetration of renewable energy," *Int. J. Electr. Power Energy Syst.*, vol. 101, pp. 255–267, 2018.
- [20] M. Wang *et al.*, "Contingency analysis considering the transient thermal behavior of overhead transmission lines," *IEEE Trans. Power Syst.*, vol. 33, no. 5, pp. 4982–4993, 2018.
- [21] Saint-Drenan *et al.*, "A parametric model for wind turbine power curves incorporating environmental conditions," *Renewable Energy*, vol. 157, pp. 754–768, 2020.
- [22] IEEE Power and Energy Society, "IEEE Standard for Calculating the Current-Temperature Relationship of Bare Overhead Conductors," IEEE Standard 738-2012, Dec 2013.
- [23] H. A. U. Khan *et al.*, "Risk-informed participation in t&d markets," *Electr. Power Syst. Res.*, vol. 202, p. 107624, 2022.
- [24] Z. Liang *et al.*, "Data-driven inverse optimization for marginal offer price recovery in electricity markets," in *Proceedings of the 14th ACM International Conference on Future Energy Systems*, 2023, pp. 497–509.

APPENDIX

A. Detailed expression for $g(\cdot)$

1) Solar heat gains are formulated as:

$$q_s = \alpha_s Q_s D, \quad (47)$$

where α_s is solar absorptivity, Q_s is total solar radiated heat intensity, D is diameter of conductor.

2) Joule heat gains are given by electric power losses as:

$$q_J = R_c I_c^2 = R_a I_c^2 + \alpha_T R_{ref} T_x I_c, \quad (48)$$

where R_c is conductor resistance at temperature T_c . R_a is DC resistance at ambient temperature T_a . α_T is temperature

coefficient of resistance and R_{ref} is DC resistance at a reference temperature, T_{ref} . We denote the difference between current and ambient temperatures as $T_x = T_c - T_a$.

3) Radiated heat losses are computed as:

$$q_r = \pi D h_r T_x \quad (49a)$$

$$h_r = \varepsilon \sigma_B (4T_A^3 + 6T_x T_A^2 + 4T_x^2 T_A + T_x^3), \quad (49b)$$

where $T_A = T_a + 273$. h_r is radiative cooling coefficient. ε is emissivity. σ_B is the Stefan-Boltzmann constant.

4) Convective heat losses are given by:

$$q_c = \pi \lambda_f N_u (T_c - T_a) = \pi D h_c T_x, \quad (50)$$

where λ_f is thermal conductivity of air. N_u is Nusselt number based on wind speed. h_c is convective cooling coefficient.

5) Dynamic Line Rating: Given the gains and losses above, steady-state DLRs can be computed as:

$$f_c^{\max} = g(T_c^{\max}) = V_c \cdot \sqrt{\frac{q_c(T_c^{\max}) + q_r(T_c^{\max}) - q_s}{R_a + \alpha_T R_{ref} T_x}}. \quad (51)$$

B. Proof of Theorem 1

We first consider the steady-state condition in (1) and consider the radiated cooling coefficient h_r . Since $T_A \gg T_x$, the last two terms of h_r can be ignored, which is $4T_x^2 T_A + T_x^3$. Then we can get our new radiative cooling coefficient:

$$h'_r = h_{r0} + k_1 T_x \quad (52)$$

$$q_r = (\pi D h'_r + \Delta r) T_x, \quad (53)$$

where $h_{r0} = 4\sigma_B \varepsilon (T_a + 273)^3$, $k_1 = 6\sigma_B \varepsilon (T_a + 273)^2$, which is independent of the conductor temperature, and $\Delta r = \pi D (4T_x^2 T_A + T_x^3)$, is a relatively small positive quantity.

Furthermore, we set $T_c = T_c^{\max}$ to get the worst-case steady-state heating balance:

$$R_{\max} I_c^2 + q_s = \pi D [h_c + h_{r0} + k_1 (T_c^{\max} - T_a)] T_x + \Delta r T_x, \quad (54)$$

where R_{\max} is conductor temperature at thermal rating T_{\max} . For simplification, we let $M_{cr} = \pi D [h_c + h_{r0} + k_1 (T_c^{\max} - T_a)]$. When near thermal rating, Joule heating is considerably more than solar heating. So we let $\Delta s = \frac{q_s}{M_{cr} I_c^2}$. Then we can get:

$$T_x = \left(\frac{R_{\max} + \Delta s}{M_{cr} + \Delta r} \right) I_c^2 \approx k_2 I_c^2, \quad (55)$$

where $k_2 = \frac{R_{\max}}{M_{cr}}$. Substituting (48), (50), (53) into (1), we can get the exact formulation:

$$[\pi D (h_c + h'_r) + \Delta r] T_x = \alpha_s Q_s D + R_a I_c^2 + \alpha_T R_{ref} I_c^2 T_x \quad (56)$$

$$[\pi D (h_c + h_{r0}) + \Delta r] T_x = \alpha_s Q_s D + R_a I_c^2 + \alpha_T R_{ref} I_c^4 \left(\frac{R_{\max} + \Delta s}{M_{cr} + \Delta r} \right) - \pi D k_1 I_c^4 \left(\frac{R_{\max} + \Delta s}{M_{cr} + \Delta r} \right)^2. \quad (57)$$

We assume the influence of Δr and Δs in (57) is ignorable. Then we quantify and compare their influence respectively. Define function $F_1(\Delta r, \Delta s)$:

$$F_1(\Delta r, \Delta s) = \alpha_T R_{ref} I_c^4 \left(\frac{R_{\max} + \Delta s}{M_{cr} + \Delta r} \right) - \pi D k_1 I_c^4 \left(\frac{R_{\max} + \Delta s}{M_{cr} + \Delta r} \right)^2 - T_x \Delta r \quad (58)$$

$$= \tilde{b}_1 \left(\frac{R_{\max} + \Delta s}{M_{cr} + \Delta r} \right) - \tilde{b}_2 \left(\frac{R_{\max} + \Delta s}{M_{cr} + \Delta r} \right)^2 - T_x \Delta r.$$

Substituting (58) into (57), we have:

$$\pi D(h_c + h_{r0})T_x = \alpha_s Q_s D + R_a I_c^2 + F_1(\Delta r, \Delta s). \quad (59)$$

Then we want to show $F_1(\Delta r, \Delta s) < F_1(0, 0) = \alpha_T R_{ref} \frac{R_{\max}}{M_{cr}} - \pi D k_1 \left(\frac{R_{\max}}{M_{cr}} \right)^2$. We conduct first order Taylor expansion at point $(0, 0)$:

$$F_1(\Delta r, \Delta s) = F_1(0, 0) + \Delta r \frac{\partial F_1(\Delta r, \Delta s)}{\partial \Delta r} + \Delta s \frac{\partial F_1(\Delta r, \Delta s)}{\partial \Delta s}. \quad (60)$$

We calculate the derivative of $F_1(\Delta r, \Delta s)$ to Δr and Δs :

$$\frac{\partial F_1(\Delta r, \Delta s)}{\partial \Delta r} = -\tilde{b}_1 \frac{R_{\max} + \Delta s}{(M_{cr} + \Delta r)^2} + 2\tilde{b}_2 \frac{(R_{\max} + \Delta s)^2}{(M_{cr} + \Delta r)^3} - T_x \quad (61a)$$

$$\frac{\partial F_1(\Delta r, \Delta s)}{\partial \Delta s} = \frac{\tilde{b}_1}{M_{cr} + \Delta r} - 2\tilde{b}_2 \frac{R_{\max} + \Delta s}{(M_{cr} + \Delta r)^2}. \quad (61b)$$

So the sufficient condition is:

$$\Delta r \frac{\partial F_1(\Delta r, \Delta s)}{\partial \Delta r} + \Delta s \frac{\partial F_1(\Delta r, \Delta s)}{\partial \Delta s} < 0, \quad (62)$$

which can be verified by numerical computation.

We then consider to impose transient process. For (54), we denote the difference between the transient T_c , given I_c and maximum values as $\Delta T = T_c^{\max} - T_c$, $\Delta I = I_c^{\max} - I_c$. Then we can reformulate the heating balance as:

$$(I_c + \Delta I)^2 R_{\max} + q_s = (M_{cr} + \Delta r)(T_c^{\max} - T_a) \quad (63)$$

$$T_x = \left(\frac{R_{\max} + \Delta s}{M_{cr} + \Delta r} \right) (I_c + \Delta I)^2 - \Delta T. \quad (64)$$

Substituting this equality into (3), we can get:

$$\begin{aligned} mc \frac{dT_c}{dt} &= \alpha_s Q_s D + R_a I_c^2 - \pi D(h_c + h_{r0})T_x \\ &\quad + \alpha_T R_{ref} I_c^2 T_x - \pi D k_1 T_x^2 - \Delta r T_x \\ &= \alpha_s Q_s D + R_a I_c^2 - \pi D(h_c + h_{r0})T_x - \Delta r T_x \\ &\quad + \alpha_T R_{ref} I_c^2 \left[\left(\frac{R_{\max} + \Delta s}{M_{cr} + \Delta r} \right) (I_c + \Delta I)^2 - \Delta T \right] \\ &\quad - \pi D k_1 \left[\left(\frac{R_{\max} + \Delta s}{M_{cr} + \Delta r} \right) (I_c + \Delta I)^2 - \Delta T \right]^2. \end{aligned} \quad (65)$$

We disregard the small terms: Δr , Δs , ΔT and ΔI . If (62) is satisfied, Δr and Δs can be neglected. Then we consider ΔT , ΔI . Define $F_2(\Delta T, \Delta I)$:

$$\begin{aligned} F_2(\Delta T, \Delta I) &= \alpha_T R_{ref} I_c^2 \left[\frac{R_{\max}}{M_{cr}} (I_c + \Delta I)^2 - \Delta T \right] \\ &\quad - \pi D k_1 \left[\frac{R_{\max}}{M_{cr}} (I_c + \Delta I)^2 - \Delta T \right]^2 \\ &= \hat{b}_1 \frac{R_{\max}}{M_{cr}} (I_c + \Delta I)^2 - \hat{b}_1 \Delta T - \hat{b}_2 \left[\frac{R_{\max}}{M_{cr}} (I_c + \Delta I)^2 - \Delta T \right]^2. \end{aligned} \quad (66)$$

Then we have:

$$mc \frac{dT_c}{dt} < \alpha_s Q_s D + R_a I_c^2 - \pi D(h_c + h_{r0})T_x + F_2(\Delta T, \Delta I). \quad (67)$$

So if we show $F_2(\Delta T, \Delta I) < F_2(0, 0) = \alpha_T R_{ref} \frac{R_{\max}}{M_{cr}} - \pi D k_1 \left(\frac{R_{\max}}{M_{cr}} \right)^2$, then Theorem 1 stands. We conduct the first order Taylor expansion at point $(0, 0)$:

$$\begin{aligned} F_2(\Delta T, \Delta I) &= F_2(0, 0) + \Delta T \frac{\partial F_2(\Delta T, \Delta I)}{\partial \Delta T} \\ &\quad + \Delta I \frac{\partial F_2(\Delta T, \Delta I)}{\partial \Delta I}. \end{aligned} \quad (68)$$

We calculate the derivative of $F_2(\Delta T, \Delta I)$ to ΔT and ΔI and get the sufficient condition:

$$\Delta T \frac{\partial F_2(\Delta T, \Delta I)}{\partial \Delta T} + \Delta I \frac{\partial F_2(\Delta T, \Delta I)}{\partial \Delta I} < 0. \quad (69)$$

Furthermore, by discretizing the time intervals, we obtain the conservative temperature evolution:

$$T_{t+1} < h(T_t, f_t) = \hat{b}'_0 + \hat{b}'_1 T_t + \hat{b}'_2 f_t^2 + \hat{b}'_3 f_t^4, \quad (70)$$

where $\mu^a = [\alpha_s Q_s D + \pi D(h_c + h_{r0})T_a] \frac{\delta t}{mc}$, $\mu^b = 1 + \frac{\pi D(h_c + h_{r0})\delta t}{mc}$, $\mu^c = \frac{R_a \delta t}{mc V_c^2}$, $\mu^d = [\alpha_T R_{ref} \frac{R_{\max}}{M_{cr}} - \pi D k_1 \left(\frac{R_{\max}}{M_{cr}} \right)^2] \frac{\delta t}{mc V_c^4}$. δt is the time interval.

C. Proof of Theorem 2

For the generator in node- i , its objective is to maximize the revenue under energy price π and reserve price τ :

$$\max_{\{p_i, R_i^{\text{up}}, R_i^{\text{dn}}\}} \pi p_i + \tau(R_i^{\text{up}} + R_i^{\text{dn}}) - c_{i,1} p_i - c_{n,2} p_i^2 \quad (71a)$$

$$p_i + R_i^{\text{up}} \leq p_i^{\max} : (\nu_i^+) \quad (71b)$$

$$p_i - R_i^{\text{dn}} \geq p_i^{\min} : (\nu_i^-), \quad (71c)$$

which is to maximize a concave problem. The partial KKT conditions can be calculated as:

$$(p_i) : -\pi + c_{i,1} + 2c_{i,2} p_i + \nu_i^+ - \nu_i^- = 0 \quad (72a)$$

$$(R_i^{\text{up}}) : -\tau + \nu_i^+ = 0 \quad (72b)$$

$$(R_i^{\text{dn}}) : -\tau + \nu_i^- = 0. \quad (72c)$$

The equilibrium for p_i and LMP_i can be reached when $\pi = \text{LMP}_i$ based on (28a), (29b), and (72b). The equilibrium for R_i^{up} , R_i^{dn} and LMRP_i can be reached according to (28b), (29b), (31), (72b) and (72c).

D. Proof of Theorem 3

For the generator in node- i , its objective is to maximize the revenue under energy price π and reserve price τ :

$$\max_{\{p, R^{\text{up}}, R^{\text{dn}}\}} \sum_t \pi p_{i,t} + \tau(R_{i,t}^{\text{up}} + R_{i,t}^{\text{dn}}) - c_{i,1} p_{i,t} - c_{i,2} p_{i,t}^2 \quad (73a)$$

$$(\nu_t^+) : p_{i,t} + R_{i,t}^{\text{up}} \leq p_i^{\max} \quad (73b)$$

$$(\nu_t^-) : p_{i,t} - R_{i,t}^{\text{dn}} \geq p_i^{\min} \quad (73c)$$

$$(\eta_t^+) : p_{i,t+1} - p_{i,t} + R_{i,t+1}^{\text{up}} + R_{i,t}^{\text{dn}} \leq U_i^{\text{up}} \quad (73d)$$

$$(\eta_t^-) : p_{i,t+1} - p_{i,t} - R_{i,t+1}^{\text{dn}} - R_{i,t}^{\text{up}} \geq -U_i^{\text{dn}}, \quad (73e)$$

which is to maximize a concave problem. The partial KKT conditions can be calculated as:

$$\begin{aligned} (p_{i,t}) : & -\pi + c_{i,1} + 2c_{i,2} p_i + \nu_i^+ - \nu_i^- - \eta_t^+ \\ & + \eta_t^- + \eta_{t-1}^+ - \eta_{t-1}^- = 0 \end{aligned} \quad (74a)$$

$$(R_{i,t}^{\text{up}}) : -\tau + \nu_i^+ + \eta_{t-1}^+ + \eta_t^- = 0 \quad (74b)$$

$$(R_{i,t}^{\text{dn}}) : -\tau + \nu_i^- + \eta_t^+ + \eta_{t-1}^- = 0. \quad (74c)$$

The equilibrium for $p_{i,t}$ and $\text{LMP}_{i,t}$ can be reached when $\pi = \text{LMP}_{i,t}$ based on (44a), (45a), and (74a). The equilibrium for $R_{i,t}^{\text{up}}$, $R_{i,t}^{\text{dn}}$ and $\text{LMRP}_{i,t}$ can be reached according to (44b), (45b), (46b), (74b) and (74c).